4

Epitaxial Graphene on SiC(0001): More Than Just Honeycombs

Lian Li
University of Wisconsin-Milwaukee, USA

1. Introduction

The growth of graphitic layers by the sublimation of Si from SiC substrates has been known since 1975 (van Bommel et al., 1975). The electronic properties of these materials are recently found to be similar to that of isolated graphene sheets (Berger et al., 2006; Castro Neto et al., 2009; Miller et al., 2009). Due to its compatibility with current standard semiconductor device fabrication technology, this process offers additional benefit of large-scale production of wafer-sized materials to facilitate the development of graphene electronics (Berger et al., 2004; Kedzierski et al., 2008; Lin et al., 2010).

Currently, 4H- and 6H-SiC polytypes are commercially available for the growth of epitaxial graphene. Because of the mismatch with the SiC, the physical and electronic properties of graphene films strongly depend on the polarity of the substrate. On the (000-1) C-face, graphene films typically grow in multiple layers with a "twisted" interface, which leads to the decoupling between different layers, and a carrier mobility comparable to that of exfoliated graphene (Hass et al., 2008a; Orlita et al., 2008; Sprinkle at al., 2009).

On the (0001) Si-face, on the other hand, the growth is self-limiting, where more uniform wafer-sized graphene films with controlled number of layers has been grown epitaxially (Emtsev et al., 2009). The graphitization has been known to start with a ($6\sqrt{3}$x$6\sqrt{3}$) (denoted "$6\sqrt{3}$" hereafter) structure, which remains at the interface during the growth of subsequent layers (van Bommel et al., 1975; Hass et al., 2008b). The interactions of this interfacial layer with the graphene above and SiC(0001) substrate below lead to giant inelastic tunnelling in scanning tunnelling spectroscopy (STS) (Červenka et al., 2010); modification of the dispersion about the Dirac point (Bostwick et al., 2007(a,b); and even gap opening in angle-resolved photoemission spectroscopy (ARPES) - a property crucial for its use in electronic devices – but found only for epitaxial graphene on the Si-face, and absent for the C-face and exfoliated graphene (Novoselov, 2007; Zhou et al., 2007).

Despite its impact on the electronic properties of graphene, the atomic structure of the $6\sqrt{3}$ layer remains controversial. Earlier studies have suggested that it consists of a graphene honeycomb layer weakly bonded to the SiC (1x1) surface (van Bommel et al., 1975; Tsai et al., 1992) or Si-rich interface layer (Northrup & Neugebauer, 1995; Forbeaux et al., 1998). More recent work indicates covalent bonding at the interface to the SiC (Seyller et al., 2008; Emtsev et al., 2008). Furthermore, most calculations, which are based on defect-free graphene covalently bonded to the SiC(0001) (1x1), indicate a metallic $6\sqrt{3}$ layer (Kim et al., 2008; Varchon et al., 2007), contrary to a semiconducting surface around K as observed in

ARPES (Emtsev et al., 2008; Seyller et al., 2008). A highly interacting graphene layer would yield a semiconducting gap (Rutter et al., 2007), but also requires Si adatoms and tetramers that are bonded to the SiC at the graphene/SiC interface, which are not seen in ARPES (Emtsev et al., 2008; Seyller et al., 2008).

By using functionalized W tips coated with transition metals such as Cr and Fe, we recently have found that scanning tunnelling microscopy (STM) imaging of the 6√3 structure close to a few meV of the Fermi level is possible (Qi et al., 2010; Rhim et al., 2011). As a result, we have observed new details of the complex electronic properties of this interfacial graphene layer that were not detected by W tips in previous studies (Hass et al., 2008b; Li & Tsong, 1996; Lauffer et al., 2008; Mallet et al., 2007; Owman & Mårtensson, 1996; Riedl et al., 2007; Tsai et al., 1992). Aided with first principles calculations, we found that the unique properties of epitaxial graphene on Si-face arise from the distinct structure of the 6√3 interfacial layer - a warped graphene layer resulted from the periodic inclusions of hexagon-pentagon-heptagon ($H_{5,6,7}$) defects in the honeycomb - to relieve the mismatch with the SiC substrate (Qi et al., 2010). The $H_{5,6,7}$ defects break the symmetry of the honeycomb, thereby inducing a gap: the calculated band structure of the proposed model along Γ-K is semiconducting with two localized states near K points below E_F, correctly reproducing the published photoemission and C *1s* core-level spectra. The 1st graphene layer assumes the defect-free honeycomb lattice; however, its interaction with the warped layer leads to deviations from the linear dispersion at the Dirac point.

On multilayer graphene films, we have found that the mismatch between the graphene and the SiC substrate can cause ridges and wrinkles, which introduce ripples in the otherwise atomically flat graphene sheet (Sun et al., 2009). These features can cause carrier scattering and decrease in mobility (Morozov et al., 2006). The origin of these ridges and wrinkles had previously been attributed to a number of causes such as the formation of carbon nanotubes (CNTs) on the surface (Derycke et al., 2002); condensation of mobile atoms that are present at the graphene/SiC interface during high temperature annealing (Luxmi et al., 2009); or compressive strain induced during cooling due to the difference in thermal expansion coefficients of graphene and SiC (Biedermann et al., 2009). We have found, by atomically resolved STM imaging, that these ridges and wrinkles are actually bulged regions of the graphene (Sun et al., 2009). We further have shown that the ridges can be manipulated, even created during STM imaging, indicating that the epitaxial graphene on SiC is still under compressive strain at room temperature (Ferralis et al., 2008; Ni et al., 2008). By minimizing this strain with decreased terrace size, nearly ridge-free graphene has been grown on vicinal SiC substrates.

2. Methods

Experiments were carried out on epitaxial graphene grown on N-doped 6H-SiC(0001), which was first etched in a H_2/Ar atmosphere at 1500 °C. After annealing at ~950 °C for 15 min in a Si flux to produce a (3x3) reconstructed surface, the SiC substrate was heated to 1100-1400 °C to grow graphene in ultrahigh vacuum (UHV) (Li and Tsong, 1996). Scanning tunnelling microscopy images were taken using W tips, as well as functionalized W tips by Fe(Cr) coating at room temperature followed by annealing at 500-700 °C in UHV (Bode, 2003; Qi et al., 2009; Rhim et al., 2011).

First-principles calculations using the Full-potential Linearized Augmented Plane Wave (FLAPW) method as implemented in *flair* (Weinert et al., 2009) model the substrate using a

3x3 6H-SiC(0001) 6-bilayer supercell, with a vacuum region of ~20-25 Å and a basis cutoff of ~195 eV. Because of the usual density functional theory underestimation of the gap (1.6 vs. 3.0 eV for 6H-SiC), comparisons of calculated density of states (DOS) and STM images are limited to biases within E_F±0.5 eV.

3. Results

3.1 STM imaging of the interface layer with W tips

Graphene growth on SiC(0001) follows the phase transitions from the Si-rich (√3x√3) (denoted "√3" hereafter), to (6√3x6√3), to 1st layer graphene (Hannon & Tromp, 2008). At the early stages, the √3 and 6√3 phases are often found to coexist; while at later stages, both the 1st layer graphene and 6√3 are observed, accompanied by pits of a few atomic layers in depth. Figure 1 presents STM images of the surface after growth at 1100 °C. The morphology is characterized by terraces of ~100 nm separated by mostly bilayer steps (Fig. 1(a)). On the terrace, two regions of different contrast are observed: a closed-pack structure in the brighter region *I*, and a honeycomb structure in the dimmer region *II* (Fig. 1(b)). Close inspection of an atomic resolution image of the structure in region *I* shown in Fig. 1(c) indicates a periodicity of 0.52 ± 0.01 nm, consistent with the (√3x√3) assignment, which consists of one Si adatom per unit cell (Northrup & Neugebauer, 1995). In addition, randomly distributed depressions are also found (circled), indicating desorption of the Si adatom at the site. Figure 1(d) is a filled-state atomic resolution image of the honeycomb structure observed in region *II*, showing that it consists of two major building blocks: two types of trimers pointing in opposite directions: marked blue are approximately 6 Å in size, and green 5 Å. These features distribute randomly without apparent order.

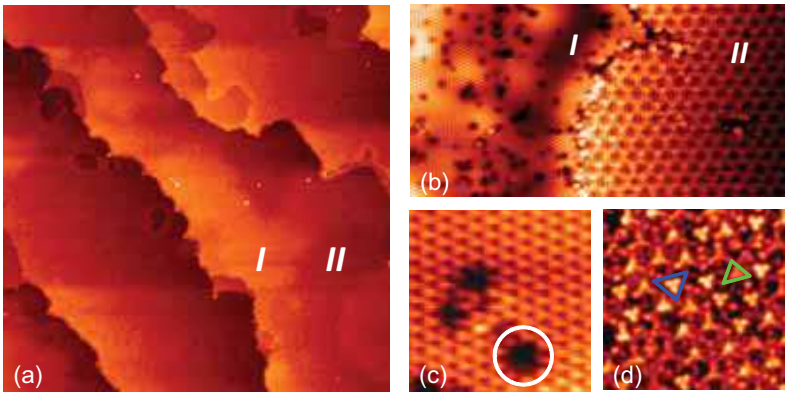

Fig. 1. (a) Topography image showing the step morphology of epitaxial graphene on 6H-SiC(0001) at 1100 °C (300x300 nm², V_s=-2.0 V, I_t=0.2 nA). (b) Close-up view of the two phases observed (50x25 nm²; V_s=-1.5V, I_t=1.2 nA). (c) Atomic resolution image of the (√3x√3) structure in region *I* (3.2x3.2 nm²; V_s=-1.5V, I_t=1.2 nA). (d) Atomic resolution image of the (6√3x6√3) structure in region *II* (12x12 nm², V_s=-1.4 V, I_t=1.2 nA).

To better understand this structure, filled- and empty-state STM images were taken, as shown in Fig. 2. Interestingly, in the empty-state image, the trimers pointing upward in filled state appear only as single bright spots, while the trimers pointing downward in filled-state now appear as featureless depressions. Note that the same trimers are identified by their relative positions to a commonly seen defect (circled).

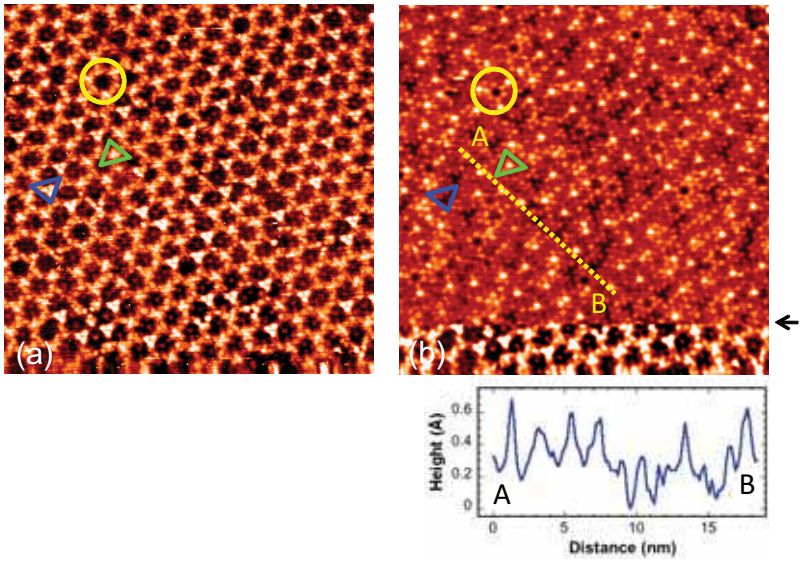

Fig. 2. STM images of the 6√3 structure taken with a W tip at the same location: (a) filled-state (35x35 nm², V_s=-1.5 V, I_t=0.3 nA); (b) empty-state (35x35 nm², V_s=+1.5 V, I_t=0.3 nA). The arrow indicates where the V_s is changed from -1.5V to +1.5V during imaging.

Small changes in heights and depressions are also observed along the line profile ***AB*** through six bright spots and three depressions in Fig. 2(b), confirming the fact that they do not line up perfectly as already evident visually. Detailed analysis of many line profiles indicates: 1) neighbouring trimers do not always fall on the same line; and 2) the spacing between the trimers is not uniform, with an average value of ~19 Å, i.e., about 6 times the (1x1) spacing of the SiC(0001) surface. These characteristics are consistent with earlier STM observations of the 6√3 structure (Li & Tsong, 1996; Lauffer et al., 2008; Mallet et al., 2007; Owman & Mårtensson, 1996; Riedl et al., 2007; Tsai et al., 1992).

Furthermore, the ratio of the larger to smaller trimers varies with growth conditions, with the later type always being more populated. For example, the ratio is found to be ~3:1 on a sample at the early stages of growth (Fig. 1(b)), where part of the surface is still covered with the √3 structure. And for a sample at later stages of growth where some regions are already converted to graphene (Fig. 2), the ratio is ~4:1.

Over all, these STM images of the 6√3 structure taken using W tips at larger bias (e.g., E_F±2.0 eV) are similar to earlier studies. Also similar is that imaging at energies closer to E_F (e.g., within ±0.1 eV) is challenging (Mallet et al., 2007; Lauffer et al., 2008; Riedl et al., 2007). Given that epitaxial graphene on SiC(0001) represents a system of a zero gap graphene supported on a wide bandgap semiconductor SiC, selective STM imaging with functionalized W tips (Deng et al., 2006), particularly near the Fermi level, may be necessary to unravel the atomic structure of the 6√3 interface layer, as discussed below.

3.2 STM imaging of the interface layer with (Fe, Cr) coated W tips

Using an Fe/W tip imaging at 1.0 eV below the E_F, the 6√3 structure appears similar to that of W tip (Fig. 3(a)). However, at E_F±0.5 eV, drastic differences are observed: the smaller up-

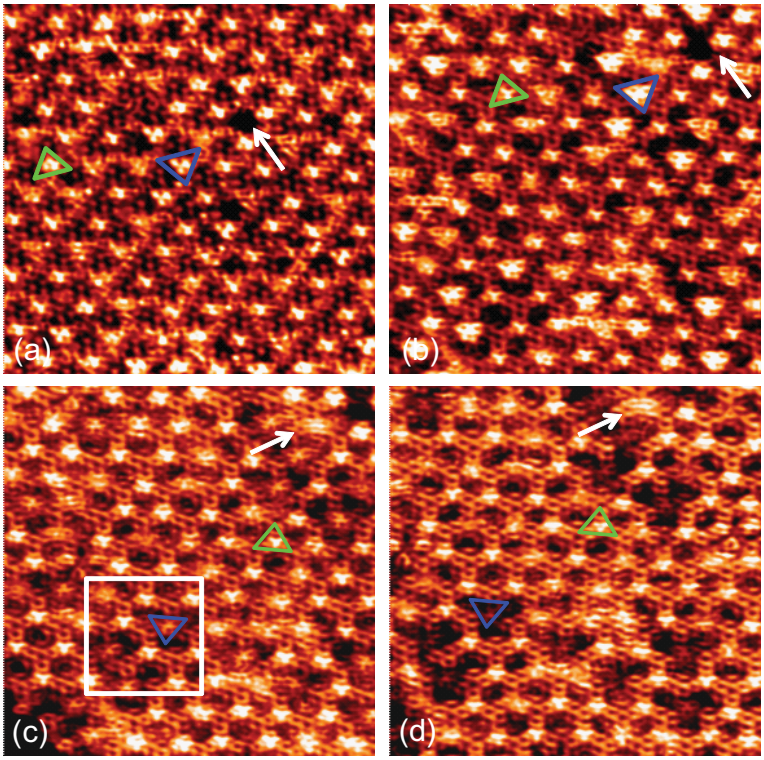

Fig. 3. Filled-stated STM images of the 6√3 structure taken with an Fe/W tip at (a) V_s=-1.0 V; and (b) V_s=-0.5 V. I_t=0.3 nA. (c) Filled-state V_s=-0.1 V; and (d) empty-state V_s=+0.1 V; I_t=0.3 nA and image sizes are 20x20 nm^2 for all.

facing trimers (marked green) now face downwards, while the larger down-facing trimers (marked blue) now appear as six-fold rosettes. Again the same trimer and rosette are identified by their relative positions to a defect marked by an arrow in both images. (Note that the two images are taken sequentially, the slight change in position is a result of thermal drift.)

Interestingly, the trimers marked by green that appear as a single protrusion in the +1.5 eV image (Fig. 2(b)), are now better resolved to be a trimer facing downwards at +0.1 eV (Fig. 3(d)). The biggest change is seen for the trimers marked blue that appear as featureless depressions in the +1.5 eV image (Fig. 2(b)): at +0.1 eV (Fig. 3(d)), they appear as rosettes surrounded by depressions. In addition, while the appearance of the trimer is independent of bias, the contrast of the rosette is slightly less in empty-state images. In the case of Cr-coated W tips, imaging down to E_F±2 meV can be carried out, with results qualitatively similar to those shown in Fig. 3 (Rhim et al., 2011).

Figure 4(a) is an STM image of the 1st layer graphene taken with an Fe/Cr/W tip. At E_F-0.052 eV, a honeycomb structure characteristic of graphene is seen over the whole surface, with additional periodic modulations. Two of the brighter ones are marked by down-pointing triangles, and two slightly dimmer ones marked by up-pointing ones. At E_F-0.52 eV (Fig. 4(b)), the honeycomb structure is no longer seen, and the features marked by

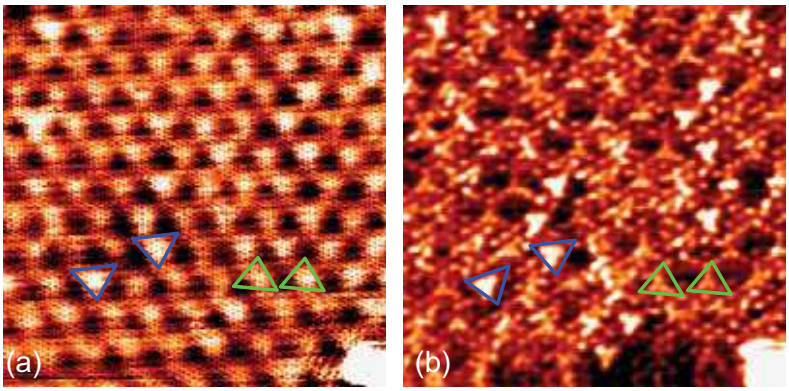

Fig. 4. STM images of the 1st graphene taken with an Fe/Cr/W tip at (a) V_s=-0.052 V; and (b) V_s=-0.52 V; I_t=5.3 nA and image sizes are 20x20 nm² for both.

triangles now appear as up- and down-pointing trimers similar to those seen by W tips (Fig. 1(d)). (Note that the large bright feature in the lower right hand corner is used to identify the features in discussion.) This confirms that the (6√3x6√3) layer remains at the interface after the growth of the 1st graphene layer, and is still accessible by electron tunnelling at 0.5 eV above and below E_F (Rutter et al., 2007).

Functionalization of W tips by transition metal coating has been typically used in spin-polarized tunnelling to probe spin dependent properties of magnetic heterostructures (Bode, 2003). The results presented here clearly show that these tips also facilitate the probing of electronic properties of the 6√3 interface layer that were not accessible using conventional W tips. To better understand this effect, we have modelled the Fe/W tips using a Fe pyramid on W(110), as shown in Fig. 5(a). The calculated density of states shown in Fig. 5(b) indicate that the apex Fe atom exhibits a large enhancement of magnetic moment (2.78 μ_B/atom) compared to that of bulk Fe, as well as the Fe atoms directly bonded to the W slab (2.1-2.3 μ_B/atom). The enhancement of magnetic moment of the topmost Fe atom is reminiscent of increased moments at surfaces and is due to a shift of peaks in DOS related to band narrowing. The minority spin channel has an especially sharp peak at ~0.5 eV below E_F (Fig. 5(b)). Electron tunnelling between graphene and these localized states enables the imaging of energy-dependent DOS not accessible with a W tip (Rhim et al., 2011).

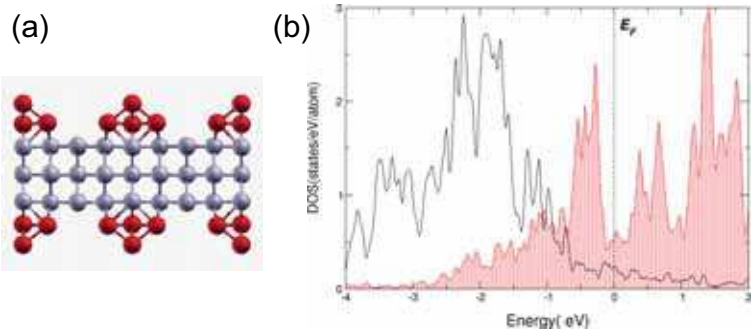

Fig. 5. (a) Ball-and-stick model used in the tip calculations. (b) Spin-resolved DOS for Fe/W(110); area shaded in red is for the minority and unshaded for the majority spins.

3.3 Proposed model of the interface layer

To account for these observations made taken with Fe/Cr coated W tips, which clearly reveal new details of the 6√3 structure, let's first consider the possible commensurate structures that can form when a layer of graphene is placed on top of the SiC(0001) (1x1) lattice. Among the possible phases, (13x13) graphene lattice is nearly commensurate to the (6√3x6√3) SiC(0001) (Tsai et al., 1992; Hass et al., 2008b), which results in two types of high symmetry positions: either a C atom or a graphene hexagon centred above a Si (Fig. 6(a)). Our calculations indicate that the in-plane graphene C-C bond is shortened from 1.67 to 1.42 Å. In addition, C atoms located directly above Si are pulled towards the SiC surface significantly such that the Si-C bond is shortened to 1.99 Å from 2.29 Å, consistent with other calculations (Mattausch & Pankratov, 2007; Varchon et al., 2008). Effectively, the graphene layer is broken.

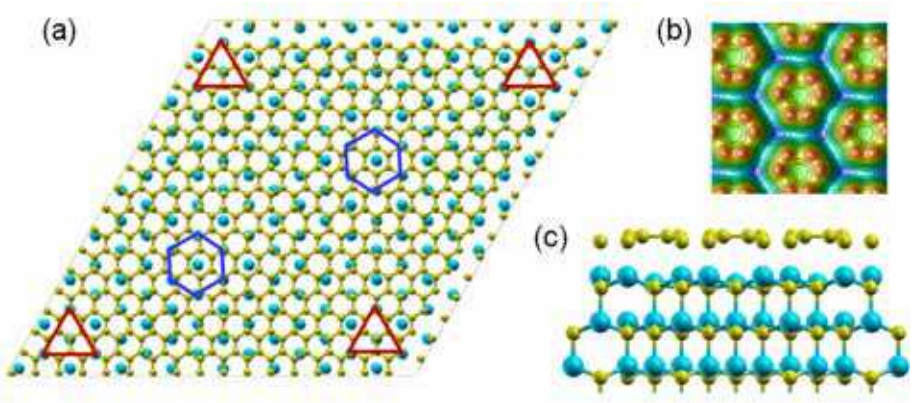

Fig. 6. (a) Ball-and-stick model of the graphene (13x13) on SiC(0001) 1x1 in plane-view (C: yellow balls; Si: blue balls). Red triangles and blue hexagons mark the two configurations of C atoms directly above Si atoms. (b) Calculated DOS at E_F+2 eV using a √3x√3 supercell and (c) ball-and-stick model in side-view, showing the distortions of the in-plane C-C bonds, and Si-C bonds at the graphene/SiC interface as a result of covalent bonding.

Alternatively, to better accommodate this bond distortion and retain the three-fold coordination for each C atom, let's now consider the inclusion of pentagons and heptagons – which cause positive and negative curvatures, respectively, when inserted into the honeycomb lattice (Charlier & Rignanese, 2001; Ihara et al., 1996). Furthermore, to preserve the long-range translational and rotational integrity of the graphene honeycomb, they can take the form of three pairs of alternating pentagons and heptagons around a rotated hexagon ($H_{5,6,7}$), which can be created by adding a C dimer to the graphene honeycomb lattice (Orlikowski et al., 1999).

As shown in Fig. 7, placement of the $H_{5,6,7}$ defects at the two high symmetry positions leads to two variants. At the "top" site, three Si atoms sit directly below the corners of the central hexagon of the $H_{5,6,7}$, with this hexagon centred above a C of the SiC substrate. At the "hollow" site, the central hexagon is centred over a Si and three Si atoms are now bonded to C atoms at the edge of the $H_{5,6,7}$ defect. Overall, this transformation decreases interfacial Si-C bonds from 6 (4) to 3 at the top (hollow) sites, further reducing the mismatch with the SiC substrate. The result is a warped graphene layer covalently bonded to SiC(0001) (1x1),

whose formation is favoured by ~0.1 eV/C compared to a perfect honeycomb structure. In addition, the top site is also found to be more stable than the hollow site by 0.03 eV/C. These results are in contrast to unsupported graphene where the $H_{5,6,7}$ defect formation energy is ~5.1 eV; the stability of the warped layer on SiC(0001) arise from its efficacy to accommodate the strain induced by the Si-C interactions at the interface. Furthermore, the spacing between the neighbouring $H_{5,6,7}$ defect sites is only approximately 6× the (1x1) lattice spacing of SiC(0001), consistent with the apparent slight disorder observed in STM images (Figs. 2 & 3).

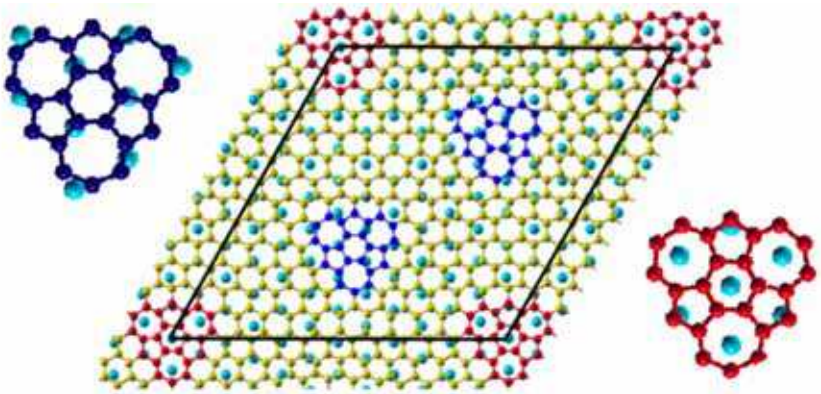

Fig. 7. Ball-and-stick model of the two placements of the $H_{5,6,7}$ defect on the SiC(0001): with the rotated central hexagon of the $H_{5,6,7}$ defect centered either above a first layer C atom (top site, marked red), or above a top layer Si (hollow site, marked blue).

To verify if these two $H_{5,6,7}$ variants on SiC would produce the complex electronic structures observed by STM, calculated local DOS isosurfaces, which resembles the STM constant current mode, are shown in Figs. 8 (a,b). For the top site, the six-fold symmetry of the centre hexagon is broken as a result of the formation of three Si-C bonds, leading to maxima at three adjacent alternating C atoms, appearing as a trimer of ~3 Å. For the hollow site variant, depressions are seen within the three heptagons as well as at the three C atoms at the tips of the three pentagons, resembling the six-fold depressions (marked by the hexagons) seen in STM. Because the six depression sites are inequivalent, they do not coincide perfectly with the hexagon of ~3 Å, also consistent with STM observations. In addition, the central three C atoms above the T_4 sites are slightly brighter, appearing as a upward trimer. Overall the main features seen in the STM images (e.g., Fig. 8(c)) at energies within E_F±0.5 eV using Fe(Cr)/W tips are well reproduced in the simulated images.

3.4 Electronic properties of the interface layer

The electronic properties of the resulting graphene structure is significantly altered due to the inclusion of the $H_{5,6,7}$ defects. Thus, experimental ARPES results provide a stringent test of our and other models. The calculated k-projected surface bands for the two $H_{5,6,7}$ variants are given in Figs. 9(a)-(c). Both variants show definite gaps, i.e., are semiconducting along Γ-K. Compared to defect-free graphene, the well-developed graphene-like σ bands are shifted to greater binding energy. Significant changes are seen in the π-band region with increased (diffuse) weight around Γ, and upward dispersing bands that do not reach E_F but are ~3 eV

below at K. In addition, there are defect-induced states (marked by arrows) with energies ε(K) of about -0.9 and -1.8 eV for the hollow and top configurations, respectively. The dispersions of these states (whose intensities decrease significantly away from K) have a tight-binding behaviour for a single band of localized orbitals, $\varepsilon(K)= \varepsilon_H$-A: the period of the oscillations seen in Figs. 9(b,c) reflect the 3x3 cell used in the calculations, while the amplitude A~0.3 eV about the "on-site" energies ε_H (indicated by the horizontal lines) is a measure of the interactions among the $H_{5,6,7}$ defects. Based on tight-binding scaling arguments, the use of larger $6\sqrt{3}x6\sqrt{3}$ (or 6x6) cells would result in a decrease in the interactions by at least an order of magnitude, i.e., we predict almost dispersionless states around K with energies $\varepsilon_H \approx$ -0.6 and -1.5 eV, in excellent agreement with the experimental values of -0.5 and -1.6 eV (Emtsev et al., 2008; Seyller et al., 2008).

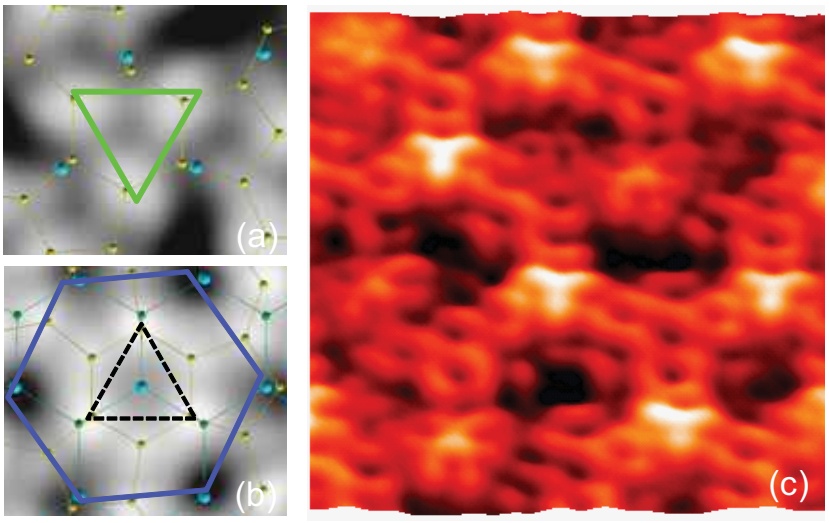

Fig. 8. Calculated DOS isosurfaces (10^{-6} a.u.$^{-3}$) for occupied states between -0.1 eV and the Fermi level for the (a) top and (b) hollow variants. Carbon and silicon atoms are represented by small and larger balls, respectively. (c) Expanded 3D STM view of the boxed region in Fig. 3(c) (5x5 nm^2).

The apparent inconsistency between a gap along Γ-K and STM imaging at very low bias can be understood by noting that STM probes the electronic states in the outer tails of the electronic distribution, whereas ARPES is sensitive to the overall wave function. In Figs. 9(d,e), the k-projected bands along Γ-M-K are shown for the two variants, but now weighted by the contributions in the vacuum region probed by STM. In both cases, the gap at K is still seen, but states elsewhere in the (1x1) zone cross E_F (such as those circled in Figs. 9(d,e)) are responsible for the contrast seen in STM images at low biases.

Calculated initial state C *1s* core level shifts, relative to C from the SiC substrate, are ~-1.1 eV for the $H_{5,6,7}$ defect, and ~-1.8 eV for the rest, which are also consistent with experimental results (Emtsev et al., 2008; Seyller et al., 2008). Overall, the warped graphene model provides a comprehensive explanation of the available experimental data on the defining properties of the $(6\sqrt{3}x6\sqrt{3})$ layer – the gap at K point, the overall dispersion, the two localized states near K, and the C core level shifts.

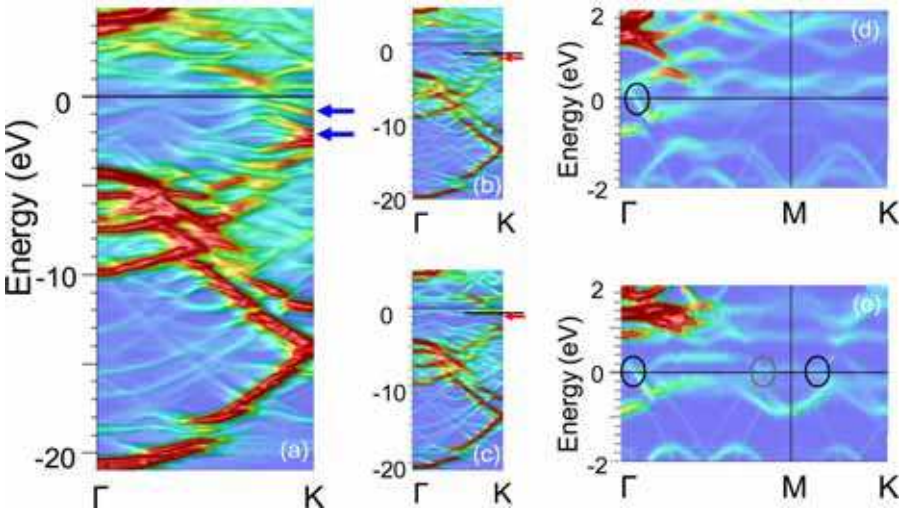

Fig. 9. Calculated k-projected surface bands (convoluted with a decaying exponential to account for the photoelectron escape depth) for the $H_{5,6,7}$ structure along Γ-K for (a) equal contributions of both variants, and (b) top and (c) hollow variants separately. Arrows mark the localized states at K and the lines in (b) and (c) indicate ε_H. Vacuum-weighted bands along Γ-M-K for (d) top and (e) hollow variants.

3.5 1st layer graphene

Calculations further indicate that the 1st layer graphene resumes the perfect honeycomb lattice with an interlayer spacing of 3.2 Å relative to the warped interface layer (Fig. 10(a)). The k-projected band structure for the interface + 1st layer graphene (Fig. 10(b)) shows almost perfect graphene bands, with the Dirac point below E_F. The bottom of the σ(π)-band at Γ is shifted upwards by about 1.3 (3.5) eV compared to the interface (Fig. 9), qualitatively consistent with the ARPES data (Emtsev et al., 2008; Seyller et al., 2008).

The downward shift of E_D = -0.4 eV indicates that the layer is n-doped, also consistent with experiment (Bostwick et al., 2007a; Zhou et al., 2007). Comparison of Figs. 10(d,e) reveals subtle, but distinct differences in the dispersions, especially above the Dirac point, as a direct consequence of the different interactions between the 1st graphene layer and the two $H_{5,6,7}$ variants. From inspection of the calculated eigenvalues and wave functions, the splitting of the Dirac states is only 33 meV. This is in good agreement with the estimated maximum value of 60 meV in one ARPES study (Bostwick et al., 2007b). Closely related is the misalignment of the bands above and below E_D, illustrated by the dotted lines in Figs. 10(c)-(e): the projections of the π states below E_D do not pass through the π* states above E_D, an observation previously attributed to electron-phonon or electron-plasmon interactions (Bostwick et al., 2007 (a,b)). Our results indicate that interactions of the π states with the $H_{5,6,7}$ defects contribute significantly to the observed dispersion at the Dirac point. Furthermore, the interactions also cause deviation from the linear dispersion of 1st graphene layer, leading to parabolic dispersion above the gap, and an apparent gap of ~0.25 eV (marked by the arrows in Fig. 10(c)), closely matched to the 0.26 eV gap assigned in separate ARPES studies (Zhou et al., 2007; Zhou et al., 2008; Rotenberg et al., 2008).

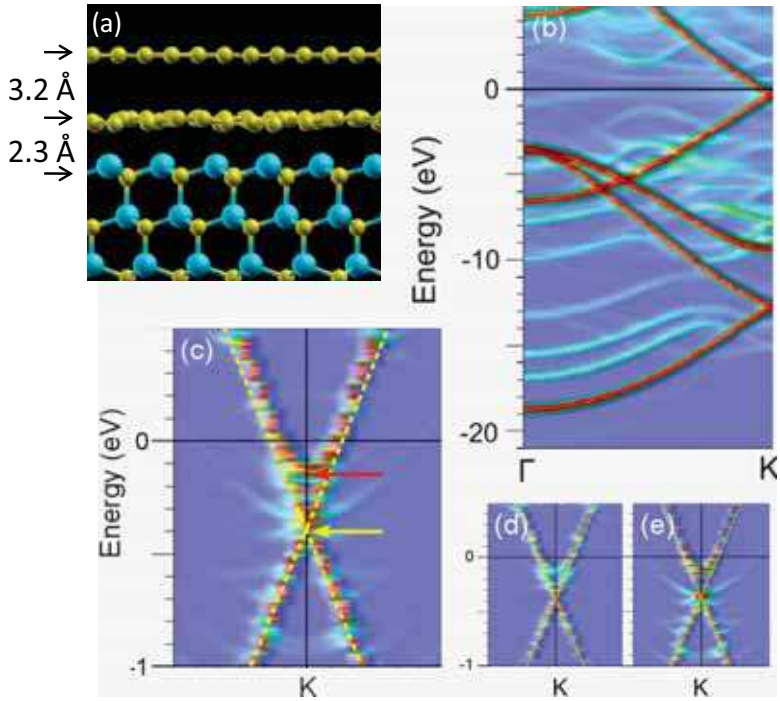

Fig. 10. (a) Ball-and-stick model, and (b) calculated k-projected surface bands of 1st layer graphene + the warped interface on SiC(0001). (c) Close-up view of bands around the Dirac point with equal contributions from (d) top and (e) hollow variants. The arrow at ~-0.4 eV marks the (split) Dirac point and dotted lines are guides for the linear dispersion.

3.6 Ridges on multilayer graphene

The morphology of the graphene grown at 1400 °C is shown in Fig. 11(a). The original SiC steps are no longer discernible. Instead, terraces with width varying from tens to hundreds of nanometers are present. On the terrace, a closed-pack lattice with a periodicity of 0.25±0.01 nm (Fig. 11(b)) is observed, indicating that multilayer graphene film is developed at this stage (Hass et al., 2008b; Lauffer et al., 2008). In addition, bright stripes along step edges and across terraces are clearly visible, with a typical size of ~1.5 nm in height and ~6 nm in width. Some of these features can terminate on a terrace, as the one circled in Fig. 11(a). Their initial density is estimated to be ~10/μm^2, though it may vary due to the creation of new ones during STM imaging (see discussion below). These features are consistent with the ridges and wrinkles reported in earlier studies (Biedermann et al., 2009; Derycke et al., 2002; Luxmi et al., 2009).

Figure 11(c) is an atomic resolution STM image of the tip of a ridge. A closed-pack lattice, same as those on the terraces, is clearly evident on top of the ridge. More importantly, no discontinuity is observed between the graphene film and the ridge both at its tip and at the boundary along either sides of the ridge. The closed-pack structure on the ridge suggests that the ridge consists of at least two graphene layers with *AB* stacking. However, the lattice constant on the ridge is measured to be 0.28±0.01 nm, slight larger than the graphene lattice

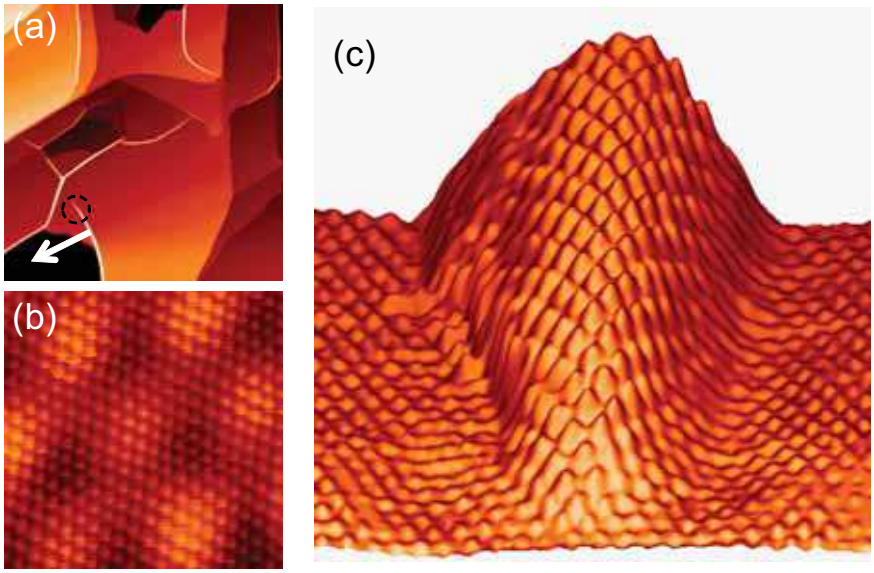

Fig. 11. (a) Topography of epitaxial graphene on 6H-SiC(0001) grown at 1400 °C taken with a W tip (1x1 μm², V_s = -2.0 V, I_t = 0.5 nA). The pit marked is 10 bilayers deep. (b) Atomic resolution image of the structure on the terrace (4.5x4.5 nm², V_s=-1.1 V, I_t=1.0 nA). (b) Atomic resolution image of the tip of a ridge in 3D view. (5x5 nm², V_s=-0.02 V, I_t=0.02 nA).

of 0.25±0.01 nm on the terrace, indicating that the lattice of the ridge is deformed due to bending. These findings clearly indicate that the ridges are neither CNTs nor domain boundaries as suggested previously (Derycke et al., 2002; Luxmi et al., 2009). They are in fact bulged regions of the graphene film, likely as a result of strain (Biedermann et al., 2009). Raman studies have indeed shown that the films are under compressive strain, which can be controlled by annealing time, reaching a theoretical limit of 0.8% (Ferralis et al., 2008; Ni et al., 2008).

In addition, we have found that their structure (e.g., length and orientation) can be manipulated by tip-surface interaction during STM imaging. In some cases, even new ridges can be created by such interactions. Shown in Fig. 12 are STM images taken sequentially at the same location, displaying the morphological evolution of the ridges. Several dramatic differences are seen. First, the ridge at location ***A*** grew much longer and now ran straight down across the whole terrace. Second, the ridge at ***B*** on the same terrace changed its direction from pointing-up to pointing-down. Third, the ridge at ***C*** along the step edge on the up terrace shrunk and became shorter. Fourth, a new ridge is formed on the up terrace at location ***D***. Lastly, a new ridge is formed at ***E*** across two terraces. Manipulation of ridges using atomic force microscopy has also been reported previously (Derycke et al., 2002), where the growth of new ridges was attributed to subsurface segments of CNTs being moved to the surface. However, since our results clearly indicate that the ridges are bulged regions of graphene film, and not CNTs, it would also rule out this particular mechanism.

Through the close examination of many STM images, it is also found that the density of the ridges varies with the size of the terrace, where fewer ridges are found on smaller terraces. The question arises then if ridge-free graphene film can be grown on a surface consists of

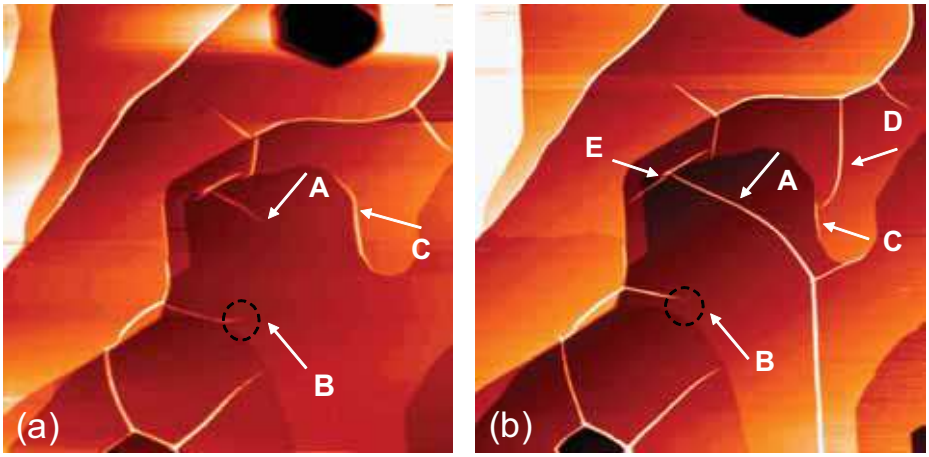

Fig. 12. STM images taken sequentially at the same location with a W tip. (a) V_s=-1.7 V, I_t=0.5 nA. (b) V_s=-2.2 V, I_t=0.5 nA. Image sizes are 1x1 μm² for both.

sufficiently small terraces, such as those of vicinal substrates. Shown in Fig. 13 is an STM image of epitaxial graphene film grown on a vicinal SiC substrate. As a result of step bunching, an average terrace width of ~80 nm is observed. Clearly, the density of ridges decreased significantly on this surface: only very few small ones are found on wider terraces, while the majority is found along the step edges. These observations indicate that the compressive strain in epitaxial graphene film is not sufficient to induce ridges on small terrace, but can still cause bending at step edges. From these results, we have estimated that a lower limit of the terrace size for ridge formation is ~80 nm.

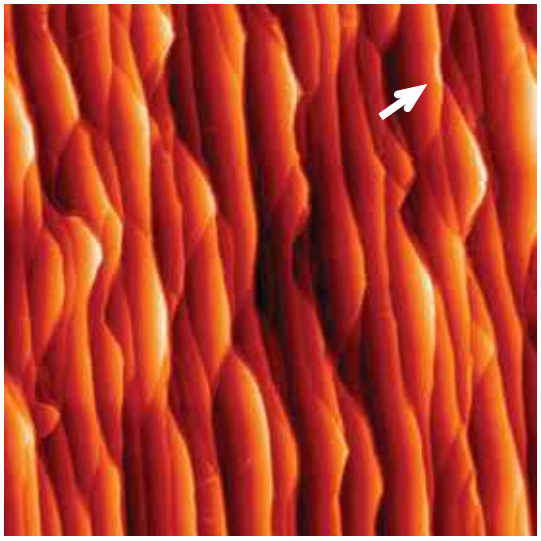

Fig. 13. STM image of epitaxial graphene film grown on vicinal 6H-SiC(0001) substrate (3.5° miscut angle), taken with a W tip (1x1 μm², V_s=-1.0 V, I_t=0.5 nA).

The picture that emerges from these results is that ridges are formed during cooling of the sample to room temperature to relieve the strain in the epitaxial graphene. On larger terraces, residual compressive strain still exists. Perturbation by the tip-surface interaction during STM imaging is clearly sufficient to initiate the creation of new ridges, as well as the growth of existing ones. Previous studies have shown that tip-surface interaction during STM imaging can exert a pressure of 5 MPa, which induces motion of subsurface dislocations on graphite (Snyder et al., 1993). The imaging conditions used in our studies are similar to those reported in these earlier studies, indicating that the pressure exerted can be of similar magnitude, sufficient to modify the ridge morphology.

4. Conclusions

In summary, using functionalized Fe(Cr) coated W tips, which facilitate the imaging of the graphene/SiC(0001) $6\sqrt{3}$ interface layer, we have found that it is a warped graphene layer resulted from the periodic inclusion of $H_{5,6,7}$ defects in the honeycomb lattice. The subsequent layer assumes the perfect honeycomb structure, though its interaction with the warped layer leads to deviations from the linear dispersion at the Dirac point. The presence of this interfacial layer alleviates the mismatch between the graphene and the SiC substrate, but also significantly modifies its electronic properties. This model provides a consistent and comprehensive explanation for the existing experimental data on the defining properties of the ($6\sqrt{3}$x$6\sqrt{3}$) layer: the gap at K point, the overall dispersion, the two localized states near K, and the C core level shifts, resolving a long-standing controversy regarding the interfacial structure of epitaxial graphene on SiC(0001).

On multilayer graphene films, we have found that ridges and wrinkles are in fact bulged regions of the graphene sheet, formed to relieve the compressive strain due to its mismatch with the SiC substrate. We can also manipulate these ridges and create new ones through tip-surface interactions during STM imaging. By minimizing this strain with decreased terrace size, nearly ridge-free graphene has been grown on vicinal SiC substrates.

5. References

Berger, C.; Song, Z.; Li, T.; Li, X.; Ogbazghi, A. Y.; Feng, R.; Dai, Z.; Marchenkov, A. N.; Conrad, E. H.; First, P. N. & de Heer, W. A. (2004). Ultrathin epitaxial graphite: 2D electron gas properties and a route toward graphene-based nanoelectronics. *J Phys. Chem. B*, Vol. 108, 19912-19916, ISSN 1520-6106

Berger, C.; Song, Z.; Li, X.; Wu, X.; Brown, N.; Naud, C.; Mayou, D.; Li, T.; Hass, J.; Marchenkov, A. N.; Conrad, E. H.; First, P. N. & de Heer, W. A. (2006). Electronic confinement and coherence in patterned epitaxial graphene. *Science*, Vol. 312, 1191-1196, ISSN 0036-8075

Biedermann, L. B.; Bolen, M. L.; Capano, M. A.; Zemlyanov, D. & Reifenberger, R. G. (2009). Insights into few-layer epitaxial graphene growth on 4H-SiC(000-1) substrates from STM studies. *Phys. Rev. B*, Vol. 79, 125411 1-10, ISSN 1098-0121

Bode, M. (2003). Spin-polarized scanning tunnelling microscopy. *Rep. Prog. Phys.*, Vol. 66, 523-582, ISSN 0034-4885

Bostwick, A.; Ohta, T.; Seyller, Th.; Horn, K. & Rotenberg, E. (2007a). Quasiparticle dynamics in graphene. *Nature Phys.*, Vol. 3, 36-40, ISSN 1745-2473

Bostwick, A.; Ohta, T.; McChesney, J. L.; Emtsev, K. V.; Seyller, Th.; Horn, K.& Rotenberg, E. (2007b). Symmetry breaking in few layer graphene films. *N. J Phys.*, Vol. 9, 385 1-22, ISSN 1367-2630

Castro Neto, A. H.; Guinea, F.; Peres, N. M. R.; Novoselov, K. S. & Geim, A. K. (2009). The electronic properties of graphene, *Rev. Mod. Phys.*, Vol. 81, 109-162, ISSN 0034-6861

Červenka, J.; van de Ruit, K. & Flipse, C. F. J. (2010). Giant inelastic tunneling in epitaxial graphene mediated by localized states. *Phys. Rev. B*, Vol. 81, 205403 1-5, ISSN 1098-0121

Charlier, J. -C. & Rignanese, G. -M. (2001). Electronic structure of carbon nanocones. *Phys. Rev. Lett.*, Vol. 86, 5970-5973, ISSN 0031-9007

Deng, Z. T.; Lin, H.; Ji, W.; Gao, L.; Lin, X.; Cheng, Z. H.; He, X. B.; Lu, J. L.; Shi, D. X.; Hofer, W. A. & Gao, H.-J. (2006). Selective analysis of molecular states by functionalized scanning tunneling microscopy tips. *Phys. Rev. Lett.*, Vol. 96, 156102 1-4, ISSN 0031-9007

Derycke, V.; Martel, R.; Radosavljević, M.; Ross, F. M. & Avouris, Ph. (2002). Catalyst-free growth of ordered single-walled carbon nanotube networks. *Nano Lett.*, Vol. 2, 1043-1046, ISSN 1530-6984

Emtsev, K. V.; Speck, F.; Seyller, Th.; Ley, L. & Riley, J. D. (2008). Interaction, growth, and ordering of epitaxial graphene on SiC{0001} surfaces: A comparative photoelectron spectroscopy study. *Phys. Rev. B*, Vol. 77, 155303 1-10, ISSN 1098-0121

Emtsev, K. V.; Bostwick, A.; Horn, K.; Jobst, J.; Kellogg, G. L.; Ley, L.; McChesney, J. L.; Ohta, T.; Reshanov, S. A.; Röhrl, J.; Rotenberg, E.; Schmid, A. K.; Waldmann, D.; Weber, H. B. & Seyller, Th. (2009). Towards wafer-size graphene layers by atmospheric pressure graphitization of silicon carbide. *Nature Mater.*, Vol. 8, 203-207, ISSN 1476-1122

Ferralis, N.; Maboudian, R. & Carraro, C. (2008). Evidence of structural strain in epitaxial graphene layers on 6H-SiC(0001). *Phys. Rev. Lett.*, Vol. 101, 156801 1-4, ISSN 0031-9007.

Forbeaux, I.; Themlin, J. M. & Debever, J. M. (1998). Heteroepitaxial graphite on 6H-SiC(0001): Interface formation through conduction-band electronic structure. *Phys. Rev. B*, Vol. 58, 16396-16406, ISSN 1098-0121

Hannon, J. B. & Tromp, R. M. (2008). Pit formation during graphene synthesis on SiC(0001): In situ electron microscopy. *Phys. Rev. B*, Vol. 77, 241404(R) 1-4, ISSN 1098-0121

Hass, J.; Varchon, F.; Millán-Otoya, J. E.; Sprinkle, M.; Sharma, N.; de Heer, W. A.; Berger, C.; First, P. N.; Magaud, L. & Conrad, E. H. (2008a). Why multilayer graphene on 4H-SiC(000-1) behaves like a single sheet of graphene, *Phys. Rev. Lett.*, Vol. 100, 125504 1-4, ISSN 0031-9007

Hass, J.; de Heer, W. A. & Conrad, E. H., (2008b). The growth and morphology of epitaxial multilayer graphene. *J Phys.: Condens. Matter*, Vol. 20, 323202 1-27, ISSN 0953-8984

Ihara, S.; Itoh, S.; Akagi, K.; Tamura, R. & Tsukada, M. (1996). Structure of polygonal defects in graphitic carbon sheets. *Phys. Rev. B*, Vol. 54, 14 713-14719, ISSN 1098-0121

Kedzierski, J.; Hsu, P. –L.; Healey, P.; Wyatt, P. W.; Keast, C. L.; Sprinkle, M.; Berger, C. & de Heer, W. A. (2008). Epitaxial graphene transistors on SiC substrates. *IEEE Trans. Elec. Dev.*, Vol. 55, 2078-2085, ISSN 0018-9383

Kim, S.; Ihm, J.; Choi, H. J. & Son, Y. –W. (2008). Origin of anomalous electronic structures of epitaxial graphene on silicon carbide. *Phys. Rev. Lett.*, Vol. 100, 176802 1-4, ISSN 0031-9007

Lauffer, P.; Emtsev, K. V.; Graupner, R.; Seyller, Th.; Ley, L.; Reshanov, S. A. & Weber, H. B. (2008). Atomic and electronic structure of few-layer graphene on SiC(0001) studied with scanning tunnelling microscopy and spectroscopy. *Phys. Rev. B*, Vol. 77, 155426 1-10, ISSN 1098-0121

Li, L. & Tsong, I. S. T. (1996). Atomic structures of 6H-SiC (0001) and (000$\bar{1}$) surfaces. *Surf. Sci.*, Vol. 351, 141-148, ISSN 0039-6028

Lin, Y. -M.; Dimitrakopoulos, C.; Jenkins, K. A.; Farmer, D. B.; Chiu, H. -Y.; Grill, A. & Avouris, Ph. (2010). 100-GHz transistors from wafer-scale epitaxial graphene. *Science*, Vol. 327, 662-662, ISSN 0036-8075

Luxmi; Nie, S.; Fisher, P. J.; Feenstra, R. M.; Gu, G. & Sun, Y. G. (2009). Temperature dependence of epitaxial graphene formation on SiC(0001). *J Elec. Mater.*, Vol. 38, 718-724, ISSN 0361-5235

Mallet, P.; Varchon, F.; Naud, C.; Magaud, L.; Berger, C. & Veuillen, J.-Y. (2007). Electron states of mono- and bilayer graphene on SiC probed by scanning-tunneling microscopy. *Phys. Rev. B*, Vol. 76, 041403(R) 1-4, ISSN 1098-0121

Mattausch, A. & Pankratov, O. (2007). Ab Initio study of graphene on SiC. *Phys. Rev. Lett.*, Vol. 99, 076802 1-4, ISSN 0031-9007

Miller, D. L.; Kubista, K. D.; Rutter, G. M.; Ruan, M.; de Heer, W. A.; First, P. N. & Stroscio, J. A. (2009). Observing the quantization of zero mass carriers in graphene. *Science*, Vol. 324, 924-927, ISSN 0036-8075

Morozov, S. V.; Novoselov, K. S.; Katsnelson, M. I.; Schedin, F.; Ponomarenko, L. A.; Jiang, D. & Geim, A. K. (2006). Strong suppression of weak localization in graphene. *Phys. Rev. Lett.*, Vol. 97, 016801, ISSN 0031-9007

Ni, Z. H.; Chen, W.; Fan, X. F.; Kuo, J. L.; Yu, T.; Wee, A. T. S. & Shen, Z. X. (2008). Raman spectroscopy of epitaxial graphene on a SiC substrate. *Phys. Rev. B*, Vol. 77, 115416 1-6, ISSN 1098-0121

Northrup, J. E. & Neugebauer, J. (1995). Theory of the adatom-induced reconstruction of the SiC(0001) $\sqrt{3}$x$\sqrt{3}$ surface. *Phys. Rev. B*, Vol. 52, R17001-R17004, ISSN 1098-0121

Novoselov, K. S. (2007). Graphene: Mind the gap. *Nature Mater.*, Vol. 6, 720-721, ISSN 1476-1122

Orlikowski, D.; Nardelli, M. B.; Bernholc, J. & Roland, C. (1999). Ad-dimers on strained carbon nanotubes: A new route for quantum dot formation? *Phys. Rev. Lett.*, Vol. 83, 4132-4135, ISSN 0031-9007

Orlita, M.; Faugeras, C.; Plochocka, P.; Neugebauer, P.; Martinez, G.; Maude, D. K.; Barra, A-L.; Sprinkle, M.; Berger, C.; de Heer, W. A. & Potemski, M. (2008). Approaching the Dirac point in high-mobility multilayer epitaxial graphene, *Phys. Rev., Lett.*, Vol. 101, 267601 1-4, ISSN 0031-9007

Owman, F. & Mårtensson, P. (1996). The SiC(0001) $6\sqrt{3} \times 6\sqrt{3}$ reconstruction studied with STM and LEED. *Surf. Sci.*, Vol. 369, 126-136, ISSN 0039-6028

Qi, Y.; Sun, G. F.; Weinert, M. & Li, L. (2009). Electronic structures of Mn-induced phases on GaN(0001). *Phys. Rev. B*, Vol. 80, 235323 1-5, ISSN 1098-0121

Qi, Y.; Rhim, S. H.; Sun, G. F.; Weinert, M. & Li, L. (2010). Epitaxial graphene on SiC(0001): More than just honeycombs. *Phys. Rev. Lett.*, Vol. 105, 085502 1-4, ISSN 0031-9007

Rhim, S. H.; Qi, Y.; Sun, G. F.; Weinert, M. & Li, L. (2011). Imaging epitaxial graphene on SiC(0001) using STM with functionalized W tips. *To be published.*

Riedl, C.; Starke, U.; Bernhardt, J.; Franke, M. & Heinz, K. (2007). Structural properties of the graphene-SiC(0001) interface as a key for the preparation of homogeneous large-terrace graphene surfaces. *Phys. Rev. B*, Vol. 76, 245406 1-8, ISSN 1098-0121

Rotenberg, E.; Bostwick, A.; Ohta, T.; McChesney, J. L.; Seyller, Th. & Horn, K. (2008). Origin of the energy bandgap in epitaxial graphene. *Nature Mater.*, Vol. 7, 258-259, ISSN 1476-1122

Rutter G. M.; Guisinger, N. P.; Crain, J. N.; Jarvis, E. A. A.; Stiles, M. D.; Li, T.; First, P. N. & Stroscio, J. A. (2007). Imaging the interface of epitaxial graphene with silicon carbide via scanning tunneling microscopy. *Phys. Rev. B*, Vol. 76, 235416 1-6, ISSN 1098-0121

Seyller, Th.; Bostwick, A.; Emtsev, K. V.; Horn, K.; Ley, L.; McChesney, J. L.; Ohta, T.; Riley, J. D.; Rotenberg, E. & Speck, F. (2008). Epitaxial graphene: a new material. *Phys. Stat. Sol. (b)*, Vol. 245, 1436-1446, ISSN 0370-1972

Snyder, S. R.; Gerberich, W. W. & White, H. S. (1993). Scanning-tunneling-microscopy study of tip-induced transitions of dislocation-network structures on the surface of highly oriented pyrolytic graphite. *Phys. Rev. B*, Vol. 47, 10823, ISSN 1098-0121

Sprinkle, M.; Siegel, D.; Hu, Y.; Hicks, J.; Tejeda, A.; Taleb-Ibrahimi, A.; Le Fe`vre, P.; Bertran, F.; Vizzini, S.; Enriquez, H.; Chiang, S.; Soukiassian, P.; Berger, C.; de Heer, W. A.; Lanzara, A. & Conrad, E. H. (2009). First direct observation of a nearly ideal graphene band structure. *Phys. Rev. Lett.*, Vol. 103 226803 1-4, ISSN 0031-9007

Sun, G. F.; Jia, J. F.; Xue, Q. K. & Li, L. (2009). Atomic-scale imaging and manipulation of ridges on epitaxial graphene on 6H-SiC(0001). *Nanotechnology*, Vol. 20, 355701 1-4, ISSN: 0957-4484

Tsai, M. –H.; Chang, C. S.; Dow, J. D. & Tsong, I. S. T. (1992). Electronic contributions to scanning-tunneling-microscopy images of an annealed β-SiC(111) surface. *Phys. Rev. B*, Vol. 45, 1327-1332, ISSN 1098-0121

van Bommel, A. J.; Crombeen, J. E. & van Tooren, A. (1975). LEED and Auger electron observations of the SiC(0001) surface. *Surf. Sci.*, Vol. 48, 463-472, ISSN 0039-6028

Varchon, F.; Feng, R.; Hass, J.; Li, X.; Ngoc Nguyen, B.; Naud, C.; Mallet, P.; Veuillen, J.-Y.; Berger, C.; Conrad, E. H. & Magaud, L. (2007). Electronic structure of epitaxial graphene layers on SiC: Effect of the substrate. *Phys. Rev. Lett.*, Vol. 99, 126805 1-4, ISSN 0031-9007

Varchon, F.; Mallet, P.; Veuillen, J. –Y. & Magaud, L. (2008). Ripples in epitaxial graphene on the Si-terminated SiC(0001) surface. *Phys. Rev. B*, Vol. 77, 235412 1-8, ISSN 1098-0121

Weinert, M.; Schneider, G.; Podloucky, R. & Redinger, J. (2009). FLAPW: applications and implementations. *J Phys.: Condens. Matter*, Vol. 21, 084201 1-14, ISSN 0953-8984

Zhou, S. Y.; Gweon, G. –H.; Fedorov, A. V.; First, P. N.; de Heer, W. A.; Lee, D.-H.; Guinea, F.; Castro Neto, A. H. & Lanzara, A. (2007). Substrate-induced bandgap opening in epitaxial graphene. *Nature Mater.*, Vol. 6, 770-775, ISSN 1476-1122

Zhou, S. Y.; Siegel, D. A.; Fedorov, A. V.; El Gabaly, F.; Schmid, A. K.; Castro Neto, A. H.; Lee, D.-H. & Lanzara, A. (2008). Origin of the energy bandgap in epitaxial graphene. *Nature Mater.*, Vol. 7, 259-260, ISSN 1476-1122

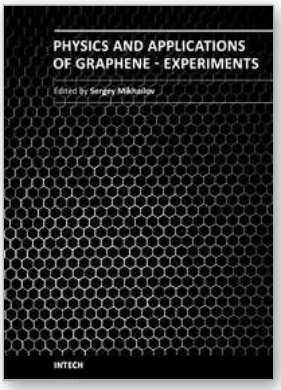

Physics and Applications of Graphene - Experiments

Edited by Dr. Sergey Mikhailov

ISBN 978-953-307-217-3
Hard cover, 540 pages
Publisher InTech
Published online 19, April, 2011
Published in print edition April, 2011

The Stone Age, the Bronze Age, the Iron Age... Every global epoch in the history of the mankind is characterized by materials used in it. In 2004 a new era in material science was opened: the era of graphene or, more generally, of two-dimensional materials. Graphene is the strongest and the most stretchable known material, it has the record thermal conductivity and the very high mobility of charge carriers. It demonstrates many interesting fundamental physical effects and promises a lot of applications, among which are conductive ink, terahertz transistors, ultrafast photodetectors and bendable touch screens. In 2010 Andre Geim and Konstantin Novoselov were awarded the Nobel Prize in Physics "for groundbreaking experiments regarding the two-dimensional material graphene". The two volumes Physics and Applications of Graphene - Experiments and Physics and Applications of Graphene - Theory contain a collection of research articles reporting on different aspects of experimental and theoretical studies of this new material.

INTECH
open science | open minds

InTech Europe
University Campus STeP Ri
Slavka Krautzeka 83/A
51000 Rijeka, Croatia
Phone: +385 (51) 770 447
Fax: +385 (51) 686 166
www.intechopen.com

InTech China
Unit 405, Office Block, Hotel Equatorial Shanghai
No.65, Yan An Road (West), Shanghai, 200040, China
中国上海市延安西路65号上海国际贵都大饭店办公楼405单元
Phone: +86-21-62489820
Fax: +86-21-62489821